JOURNAL OF MATERIALS SCIENCE 26 (1991) 6789–6799

Fracture behaviour of a TiB_2-based ceramic composite material

M.K. BANNISTER*, M.V. SWAIN
Advanced Materials Technology Centre, Mechanical Engineering Department, University of Sydney, Sydney NSW 2006, Australia

The fracture behaviour of a multicomponent TiB_2/BN/AlN material was studied in both the double cantilever beam (DCB) and single-edge-notched beam (SENB) geometries. Crack growth in the SENB geometry at various stages of the test was monitored using optical and electron microscopes. R-curve behaviour was found in both specimen geometries for this material. Evidence of crack–interface tractions were found in the form of (i) ligamentary bridges and (ii) frictional interlocks, along with evidence for microcracking about the crack tip. Measurements of crack-opening displacement with distance back from the crack tip were made. The inflection point of such data is in agreement with the range of the measured *R*-curve.

1. Introduction

The origin of the increase in fracture resistance with crack growth, illustrated by the "R-curve" function (a concept borrowed from the fracture behaviour of metals [1]), has been the subject of discussion and research for a number of years. This behaviour is seen in a wide variety of materials: metals, ceramics, concrete, rocks, composites, etc., and it is becoming apparent that the mechanism responsible for the crack-growth resistance may be a combination of factors, some of which dominate in certain materials [2–7].

In zirconia-based ceramics, transformation toughening has been established as the principal cause of crack resistance. This is also the case for other materials capable of martensitic transformations [7]. However, this mechanism can only be applied to a small class of materials, whilst R-curve behaviour can be seen in materials which are unable to undergo transformation toughening. Thus, alternative processes must be occurring by which these materials are toughened.

A number of mechanisms have been proposed for improving the fracture toughness of ceramics and the development of R-curve behaviour. Microcracking has long been proclaimed as a mechanism for increasing the toughness of ceramics, and apart from a relatively limited subset of materials such as some rocks and zirconia-toughened alumina [8, 9], there is very little direct experimental support for such a toughening concept. However, recent theories by a number of authors [10–12] do suggest the occurrence of a toughening increment associated with the development of a partially and fully saturated microcrack zone about the crack tip. The toughening increment anticipated from such theories is very modest. Instead, there is increasing evidence to support the concept of crack tip shielding via the formation crack bridging ligaments which contribute to improved toughness and associated R-curve behaviour.

An experiment by Knehans and Steinbrech [13] has been cited as evidence for the microcracking zone model. In their experiment, Knehans and Steinbrech grew cracks through several millimetres in alumina specimens, recording strong rising R-curves. They then removed the crack-path material up to the crack tip by saw-cutting. On regrowing the crack, the resistance was measured to be that originally at the start of the R-curve. These results imply that the toughening process occurs in the crack wake and thus can be argued to support the microcracking model. However, other mechanisms are also possible for the source of toughening, these will be outlined later. We note that the existence of the microcracked zone in its theoretical shape has not yet been conclusively proven, and its effect on the crack tip is still a matter of conjecture. However, recent observations by Lutz *et al.* (personal communication), on a dispersed pressure zone composite material, show clear evidence for a genuine microcracked zone about the crack tip.

Other theories that have been advanced for the observed rising crack resistance include crack restraint by pinning and bowing, and by crack deflection and twisting, although all these are non-cumulative mechanisms and thus do not explain the large crack extension range over which the R-curve rises in many materials [2].

Another possible explanation for crack-growth resistance is the concept that there exists some physical restraining force across the newly formed crack interface. Here the effect of the restraining forces is to act against the applied load and thus lower the net stress intensity factor at the crack tip. This theory has been used by Mai and co-workers [3] to model the

*Present address: Department of Materials Engineering, University of California, Santa Barbara, USA.

0022–2461/91 $03.00 + .12 © *1991 Chapman & Hall*

R-curves for fibre-reinforced cement materials in which the restraining force was produced by the pull-out of the reinforcing fibres from the cement matrix. It was further developed by Mai and Lawn [14] and used in conjunction with experimental observations [2] to model the R-curve behaviour for a coarse-grained alumina. Here the restraining force was observed to be from bridging alumina grains along the crack path. Further support for this model is available in the work of Swanson [4, 15] who studied crack propagation in rocks (in particular Westerly granite), alumina, and glass ceramics. In his work, ultrasonic and *in situ* microscopy investigations showed the presence of two principal restraining mechanisms operating behind the visually defined crack tip. These were (i) frictional or geometrical interlocking of microstructurally-rough fracture surfaces; and (ii) ligamentary bridging by intact islands of material left behind the advancing fracture front. A number of theories have been recently developed to model the crack closure ligaments on the crack-tip stress-intensity factor [14, 16]. The simplest basis for considering the situation of the balance of the opening or applied stress intensity, and of closure or bridging, or another crack-tip energy-absorbing process, is

$$K_a(c) = K_0 + K_b(c) + K_m(c)K_i \quad (1)$$

where K_0 is the intrinsic toughness of the material, $K_b(c)$ is the crack-tip bridging-closure stress intensity, $K_m(c)$ is the microcrack contribution to toughening, and K_i are other possible contributions to the total toughness. Bennison and Lawn [25] attempt to distinguish between intrinsic and extrinsic (bridging) contributions to the toughness by letting K_0 in Equation 1 equal T_0 the intrinsic grain-boundary toughness of the single-phase polycrystalline alumina material they examined. For a complex heterogenous material with many interfaces and phases, such an approach is more difficult to justify. An alternative approach is to calculate the crack resistance ($J\,m^{-2}$) usually from the relationship ($J = K^2/E$).

Knehans and Steinbrech's [13] results have been explained in terms of crack–interface bridging mechanisms. As the crack grows, the crack resistance also increases as more bridging sites are formed. The plateau in the R-curve is reached when the equilibrium number of bridging sites is produced along the crack path behind the tip [3, 14]. Removal of the material behind the crack tip by saw-cutting destroys the bridging sites and lowers the material's crack growth resistance to its original value.

In reality, the closure forces bridging of the crack to act at discrete points; therefore K_i should be calculated as a sum for the individual forces. However this becomes tedious as the number of restraining sites increases. Thus Mai and Lawn [14] approximate the sum of the discrete forces $F(x)$ (x = distance back from the crack tip) by an integration over continuously distributed stresses $p(x) = F(x)/d^2$ where d is the mean separation between closure force centres. As the front grows, bridging sites are activated and remain active until at some critical crack dimension C^*, rupture of the sites most distant from the crack front occurs. Thereafter a steady-state zone of bridging (length C^*) translated with the growing crack K_i can now be expressed by the Green function solution

$$K_i = \int \bar{G}(c, x)p(x)dx \quad (2)$$

where $p(x)$ is the closure stress function, and $\bar{G}(c, x)$ the appropriate Green function for the specific geometry used.

Equation 2 may then be rearranged to give the integral in terms of $u(x)$: the crack opening displacement (COD). Here Mai and Lawn [14] sacrifice accuracy in order to obtain simple, convenient working equations by neglecting the effect that the closure stresses have on $u(x)$. A proper treatment of the situation leads to a non-linear integral equation [14] for which no analytical solutions are available; thus an involved iterative process [3] must be used for exact solutions to be calculated.

The closure stress function, now $p(u)$, is completely determined by the micromechanics of the bridging site rupture process. Mai and Lawn [14] suggest that for frictional pull-out of interlocking grains, this is given by

$$p(u) = p^*(1 - u/u^*)^m \quad (3)$$

where p^* is the limiting value of stress, u^* is the characteristic rupture separation, and m is an exponent.

The theory eventually generates the effective toughness function for a crack originating from a starter notch

$$K(\Delta c) = K_0(\Delta c < d) \quad (4a)$$

$$K(\Delta c) = K_\infty - (K_\infty - K_0)\left[1 - \left(\frac{\Delta c - d}{\Delta c^* - d}\right)^{1/2}\right]^{m+1} (d \leqq \Delta c \leqq \Delta c^*) \quad (4b)$$

$$K(\Delta c) = K_\infty(\Delta c > \Delta c^*) \quad (4c)$$

where Δc = crack growth.

$$K_\infty = K_0 + Ep^*u^*/(m + 1)K_0 \quad (5)$$

The critical crack growth for bridge rupture, Δc^*, is thus

$$\Delta c^* = d + (\pi Eu^*/22^{1/2}\psi K_0)^2 \quad (6)$$

where ψ = numerical crack geometry term $\simeq \pi^{-1/2}$.

More recently, Majumdar *et al.* [17] have approached the analysis of R-curve development in non-phase-transforming ceramics from a slightly different perspective. They propose the R-curve is a consequence of restraints due to ligaments which may be approximated by a uniform closure stress σ_0. This approach is mathematically equivalent to the Dugdale [18] strip-yield model that has been successfully applied to steels and polymers. The resulting expression for the toughening increment (equivalent to Equation 4b above) is

$$K(\Delta c) \simeq (22^{1/2}/\pi^{1/2})\sigma_0(a - c)^{1/2} \quad (7)$$

where c is the crack length and a–c is the bridging length. These authors have also developed an expression for the crack-opening displacement with distance

from the crack tip for an infinite centre-cracked strip. Profiles based on such an analysis are different from the anticipated parabolic shape and show a distinct inflection at the end of the bridging zone.

The aim of this work is to observe the mechanisms responsible for toughening and R-curve behaviour for the T_iB_2 composite and compare with the concepts outlined in the crack–interface bridging theory above.

2. Experimental procedure

The material investigated was from a multicomponent system containing approximately 50% TiB_2, the remaining 50% consisting of a mixutre of BN and AlN. It is used as an evaporation source for resistance-heated vacuum aluminium metallizers, due to its electrical conductivity, wettability by molten aluminium, and good thermal shock resistance [19, 20]. This thermal shock resistance is attributable to the presence of BN which exists as a graphite-like, flake structure that readily cleaves under stress. Thus the TiB_2/BN/AlN materials can accommodate stresses induced by severe thermal gradients by microcrack growth, leading to significant non-linear stress–strain behaviour [20].

The relatively easy fracture and flake-like nature of the BN component suggests that any microcracking associated with the propagating crack might be evident within this phase. Two specimen geometries were used to gather fracture data during stable crack propagation, the double cantilever beam (DCB) and single-edge-notched beam (SENB) specimens.

2.1. Single-edge-notched beam

Specimens were tested in the SENB geometry in three-point loading, in a universal testing rig at a cross-head speed of 0.05 mm min^{-1}. Load (F) was measured by a load cell and the crack-opening displacement (COD) was measured by a clip gauge extensometer.

Before the fracture tests were begun, it was necessary to polish the specimen faces on a tin lap and then to deposit a gold coating on them in order for the crack to be highlighted. The specimens were loaded until crack growth occurred, then unloaded and the crack length measured under an optical microscope. The critical stress-intensity factor as a function of crack growth (here called $K(\Delta c)$) was calculated from the measurements of load required to propagate the crack [21] and plotted to give the R-curve. A typical load COD curve is shown in Fig. 1.

One specimen was also examined under the SEM at various stages of its crack growth in order to investigate the possible existence of a microcracking zone or crack–interface bridging sites. In both optical and SEM observations, the crack was wedged open in order that the crack tip and any microcracking present might be discernable. Unfortunately crack-length measurement was difficult due to the uncertainty in the crack-tip position. For consistency, this was taken as the point at which the crack was no longer observable under an optical microscope (magnification $\times 600$).

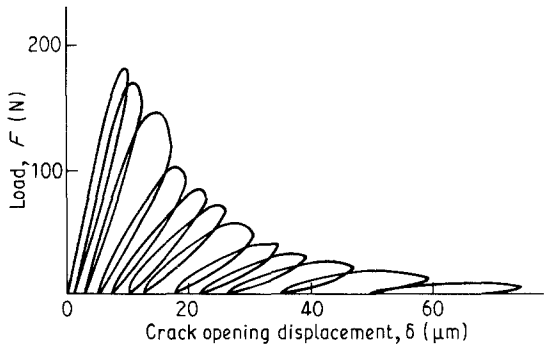

Figure 1 An example of the crack-opening displacement nervous load during stable crack extension of an SENB specimen in three-point flexure.

2.2. Double cantilever beam

The DCB specimen was tested in a similar fashion in a universal testing rig at a cross-head speed of 0.05 mm min^{-1}. Load (F) and COD were measured by a load cell and clip-gauge extensometer, respectively and recorded on an X–Y plotter. Crack lengths were calculated using measured compliances and theoretical compliance against crack-length functions which had been corrected to account for deviations from beam theory [21].

The specimen was loaded until substantial deviation from linearity was observed on the F against COD plot. It was then partially unloaded to allow measurement of specimen compliance, after which the procedure was repeated.

The specimen eventually fractured through one of the moment arms, no guiding groove having been used in order to eliminate any possible interaction of the crack with the groove walls [4]. Again, the critical stress-intensity factor was calculated from the crack-propagation load and plotted to give the R-curve.

3. Results

3.1. Single-edge-notched beam

3.1.1. Visual investigation

The typical crack path in one of the SENB samples is shown in optical micrographs in Fig. 2. The light-coloured particles are TiB_2, the darker areas being the BN/AlN mix. It is evident that the very tortuous path taken by the crack lies for the most part within the BN/AlN 'matrix phase' (Fig. 3). This is due to the flake-like nature of the BN, which fractures easily and acts as a crack guide (Fig. 4). This behaviour is also seen on the fracture surfaces of specimens (Fig. 5). The flake-like structure of the BN/AlN matrix can clearly be seen and contrasts markedly with the relatively 'clean' fractures of the TiB_2 grain. Other areas support the microcracking zone theory due to the ease with which the BN/AlN matrix cleaves (Fig. 6). The stresses surrounding the crack tip might easily cause the matrix to cleave, within a restricted zone (mean free path) between the TiB_2 particles, producing microcracks which will increase the fracture resistance of the specimen [5].

During fracture, the crack was not constrained to one particular path (Fig. 7). Branches in many cases

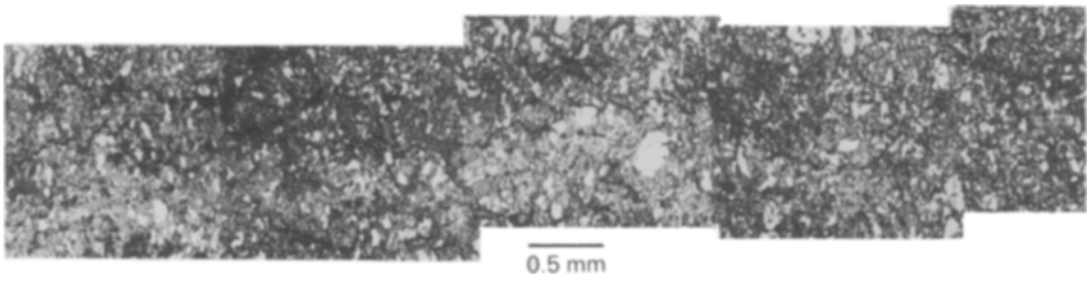

Figure 2 Optical micrograph of a crack extended in the TiB_2/BN/AlN composite material with the SENB method.

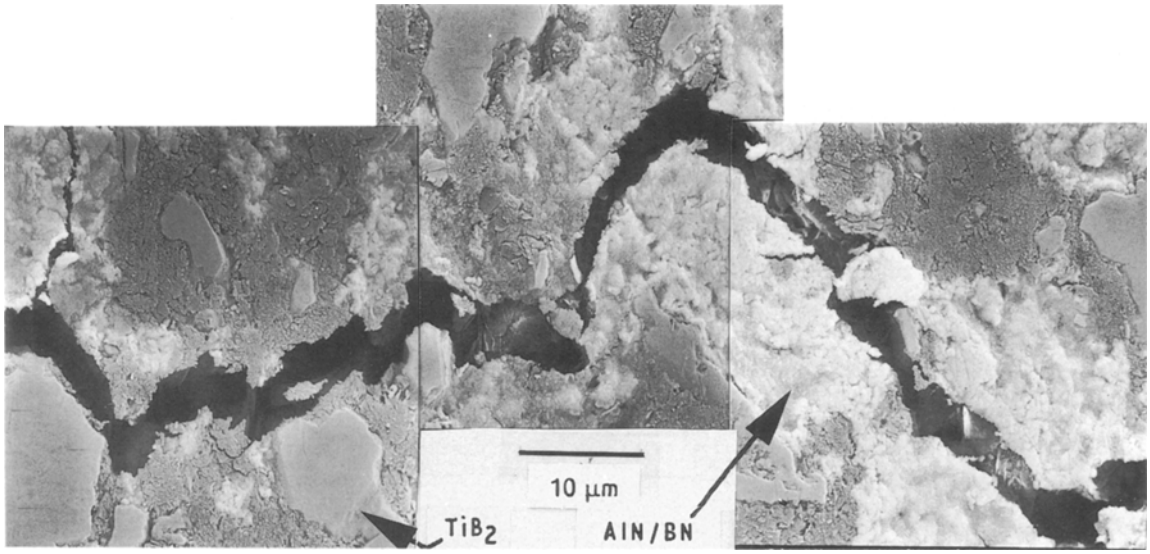

Figure 3 Scanning electron micrograph indicating the very tortuous crack path in the TiB_2-based composite. The smooth particles are TiB_2 grains and the remaining material is the BN/AlN matrix phase.

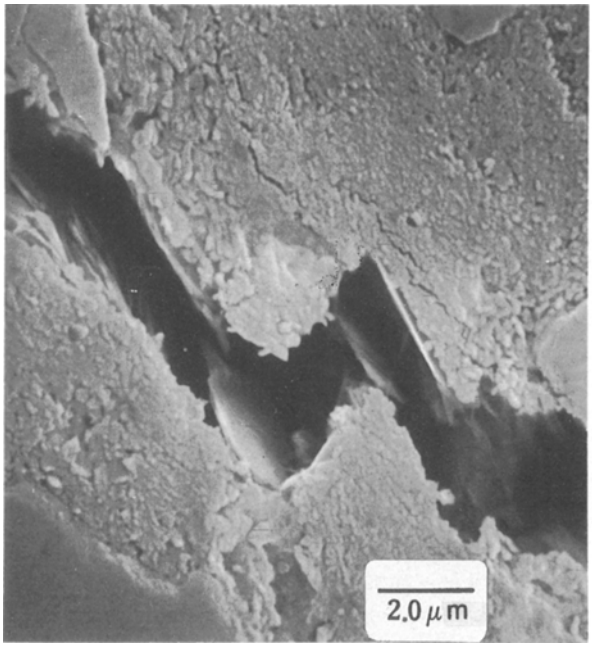

Figure 4 Scanning electron micrograph showing the flake-like structure of the BN material and how it influences crack behaviour.

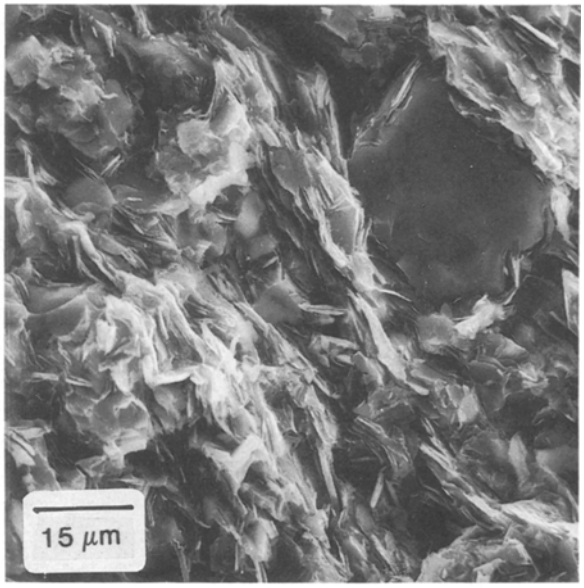

Figure 5 Scanning electron micrograph of the fracture surface of the composite material illustrating the flake structure of BN and its influence on fracture behaviour.

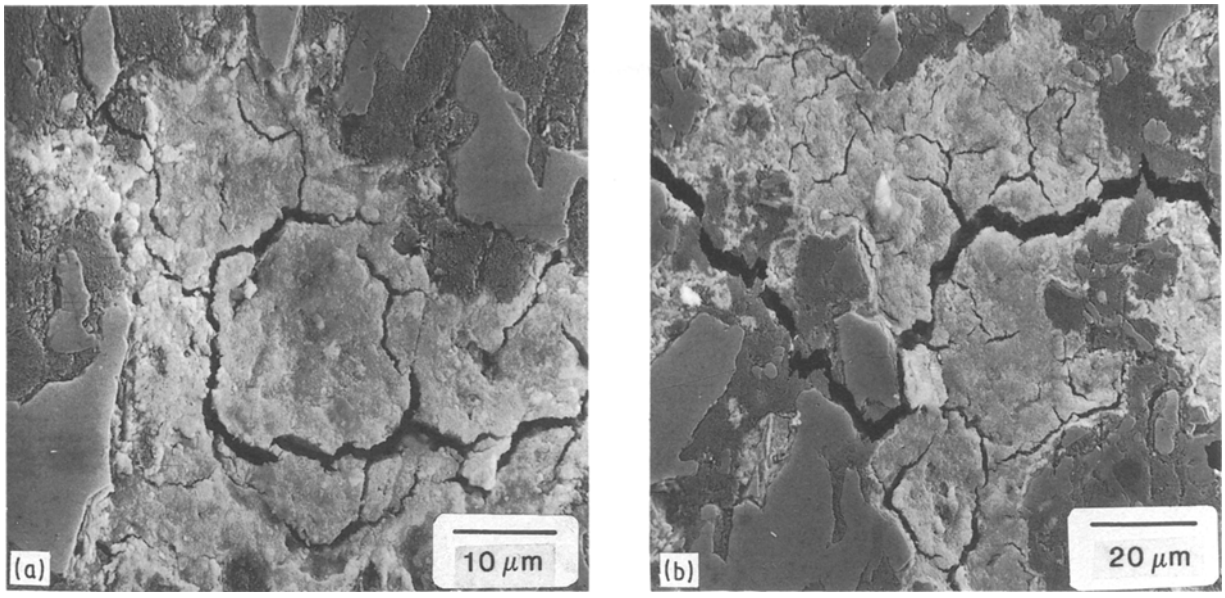

Figure 6 Example of microcracking within the BN/AlN matrix phase about the crack tip. Note that this microcracking appears to be constrained between the TiB_2 grains.

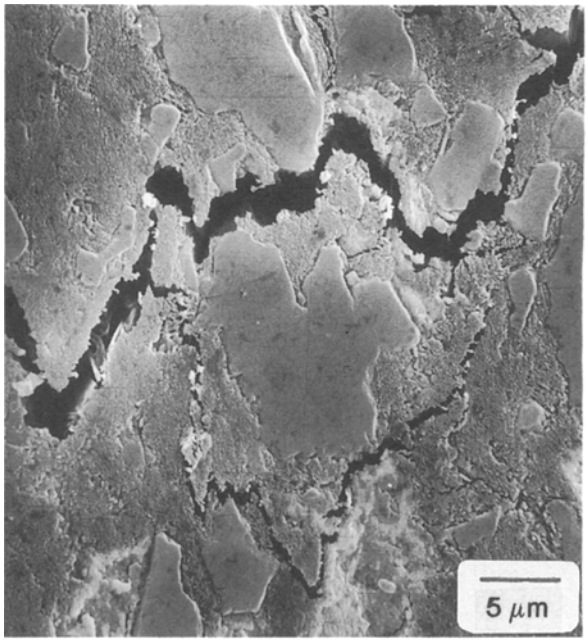

Figure 7 Scanning electron micrograph illustrating crack branching along the crack path.

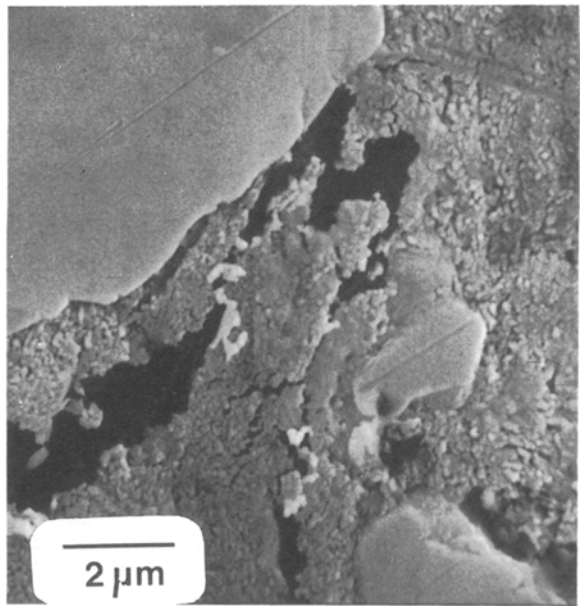

Figure 8 Scanning electron micrograph showing the very significant crack front deflections during its passage through the composite.

were produced from the main crack and these would act as effective energy sinks for the fracture process. In many cases (Figs 7 and 8) the crack was seen to grow at right angles to the general propagation direction. Although this behaviour is most probably caused by the crack following directions of least energy expenditure, these deflections would have the effect of changing the fracture from mode I to mode II and/or mode III.

The complicated crack path produced by the microstructure allowed crack–interface tractions to be set up. Fig. 9 shows ligamentary bridges formed at various stages during the test. These are formed as the material fractures beneath the surface on the most energetically favourable planes (compared to the development of 'hackles' noted by Swanson [15]). This leaves intact islands of material bridging the crack and thus setting up restraining forces behind the advancing fracture front. These restraining forces will remain active until the crack opening displacement is sufficiently large to cause microfracturing of the ligamentary bridges.

Fig. 10a illustrates frictional interlocks being formed by the complicated crack path. Here, restraining forces are set up behind the crack tip by interlocking of the geometrically rough crack faces. Again, these sites will remain active, contributing to the specimen's crack-growth resistance, until microfracturing occurs. This is shown in Fig. 10b, where microcracks are being formed by the frictional forces present at the bridging site. These microcracks will grow until the bridging site is destroyed.

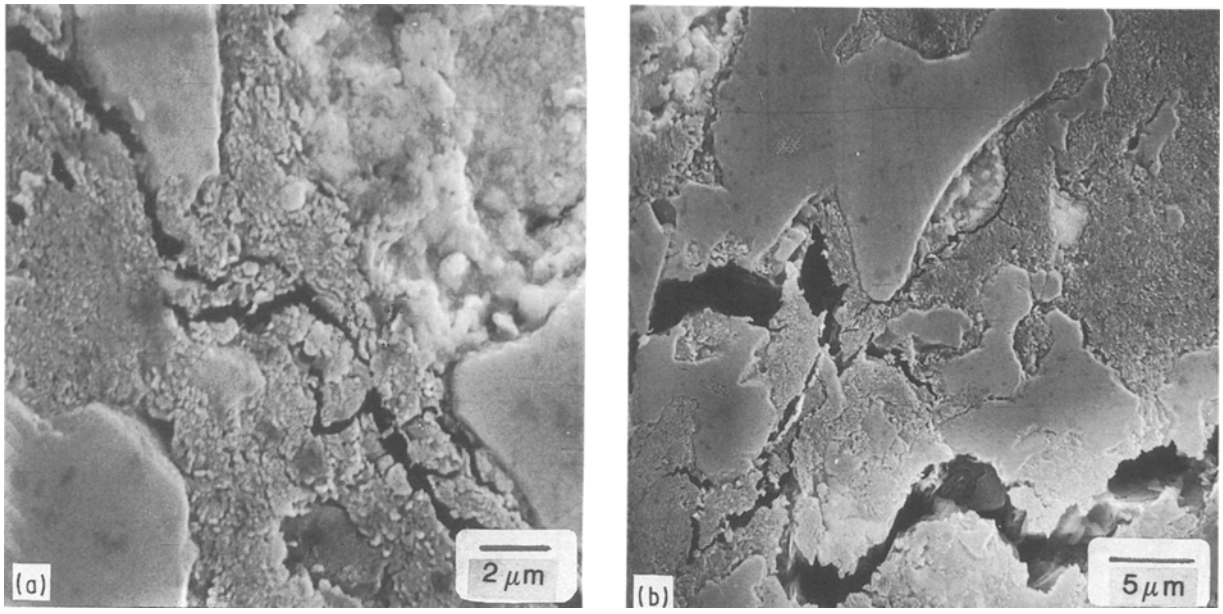

Figure 9 Two scanning electron micrographs, showing the formation of ligamentary bridges behind the crack tip on (a) fine and (b) coarse scale.

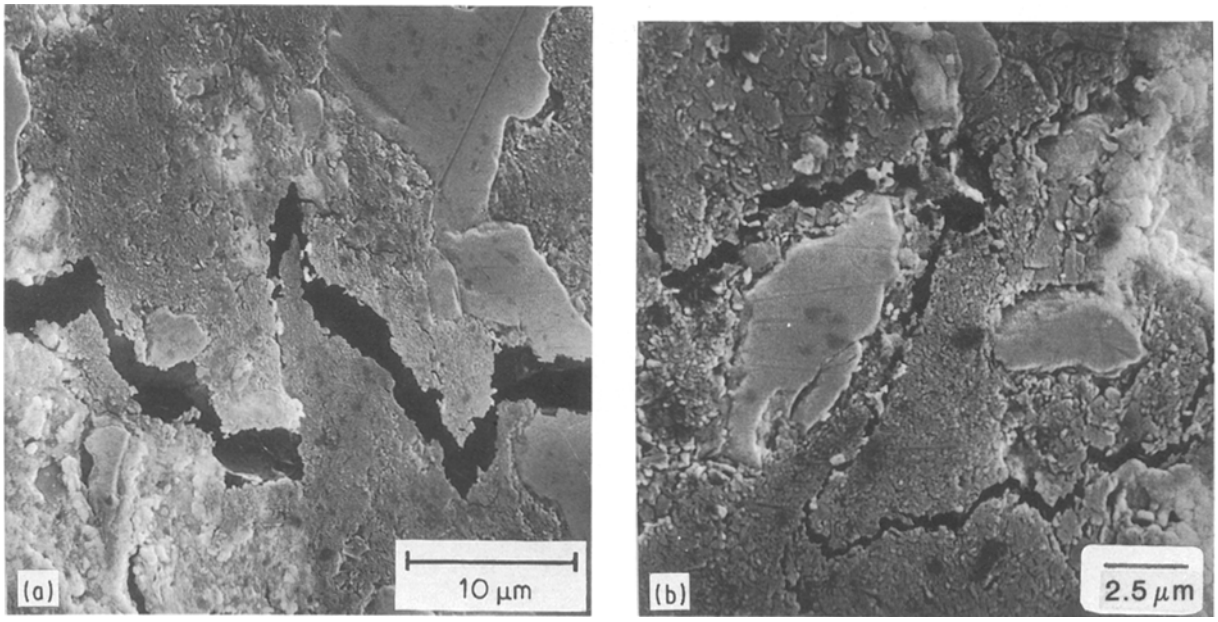

Figure 10 Scanning electron micrograph of the development of frictional interlocks due to the crack-path tortuosness.

The debris formed by the destruction of these bridging sites can also contribute to the crack–interface tractions. Fig. 11 shows debris which has lodged within the crack, which will lead to an increase in the frictional forces between the crack faces. Both the frictional forces, microcracking and debris formation, prevent crack closure upon unloading the accounts for the residual COD opening in Fig. 1.

Investigation of one SENB sample with the SEM showed there to be approximately 60 active bridging sites operating up to 1.35 mm behind the crack tip. The sites were not uniformly distributed throughout the interaction length, but were biased towards the crack tip, an observation that tends to support the stress distribution presented by Mai and Lawn [14]. Note that this is only an estimate of bridging site numbers, due to the uncertainty in determining whether or not a site is active. The crack-opening displacement 1.35 mm behind the crack tip, when the crack propagation length was 3.26 mm, was measured to be 1.7 μm. Therefore in the nomenclature defined above, we have

$$\Delta c^* = 1.35 \times 10^{-3}\ \text{m}$$
$$d = 2.37 \times 10^{-5}\ \text{m}$$
$$u^* = 1.7 \times 10^{-6}\ \text{m}$$
$$E = 111.3\ \text{GPa}\ [19]$$

Earlier, when the crack had propagated approximately 2.83 mm, scanning electron micrographs were taken along the crack length. These were used to

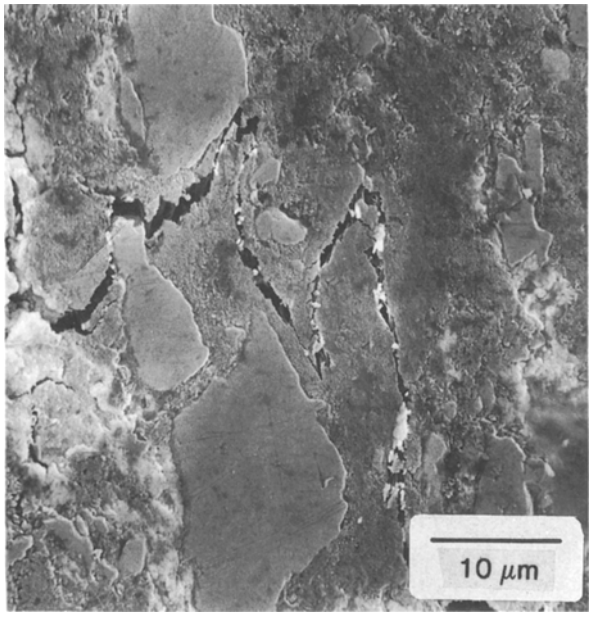

Figure 11 Scanning electron micrograph illustrating the formation of debris at the frictional interlocks.

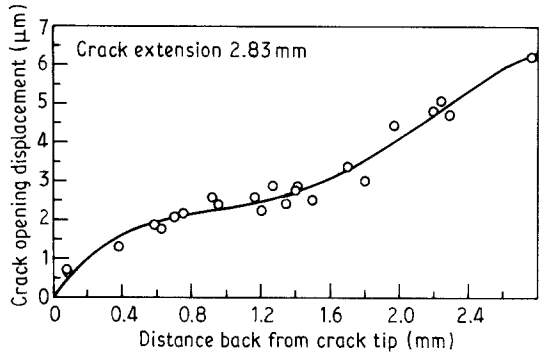

Figure 12 Measurement of crack opening displacement (COD) gains distance back from the crack tip. These observations were measured from a fully wedged opened crack in an SENB specimen. The specimen thickness, width and span were 5.86, 2.32 and 46.40 mm, respectively. The initial notch was 1.13 mm deep and the crack had been extended 2.83 mm.

estimate the crack-opening displacement (COD) as a function of distance from the crack tip (Fig. 12). This profile has a marked inflection at ~1.4 mm from the crack tip, and is not as expected from theory [23] which predicts a parabolic profile. Note that at the end of the 'plateau' region the distance from the crack tip is approximately 1.3 mm. This corresponds closely to the interaction zone length for the active bridging sites. Thus the data suggest that the observed crack profile is due to the action of crack–interface tractions behind the crack tip. These tractions have the effect of lowering the net stress intensity factor seen by the crack tip (crack-tip shielding), thus a greater external load must be applied in order to propagate the crack. In an effort to overcome the crack–interface tractions and achieve the same critical conditions at the crack tip, the greater external applied load will act to increase the COD far behind the tip, again seen in Fig. 12. The profile of the COD with distance from the crack tip bears a strong resemblance to that proposed by Majumdar et al. [17].

Tada [23] gives theoretical expressions relating stress distributions to COD and stress intensity factors. Assuming a constant stress distribution over the interaction zone length ($m = 0$ in Equation 3, as used before with Mai and Lawn's theory [14]), we can estimate the required stress level needed (which is applied to overcome the internal tractions) to account for the difference between the measured and theoretical CODs. Using this value of the stress level, we can estimate the addition it will make to the critical stress-intensity factor and thus make a comparison with the increase measured from the R-curve. Now

$$\text{COD} = \frac{8pb}{\pi E} \tag{8}$$

where p = stress level; b = interaction zone length (= 1.35 mm); E = 111.3 GPa; and COD = 0.62 μm. This gives us p = 20.1 MPa.

Considering the approximations used, this compares favourably with the values of p^* obtained earlier using Mai and Lawn's theory [14]. Using the above value of p (20.06 MPa) it is now possible to calculate the toughening increment.

$$\Delta K_I = 2/\pi(p2^{1/2}\pi b) \tag{9}$$

Thus here $\Delta K_I = 1.18$ MPa m$^{1/2}$ (c.f. measured $\Delta K_I = 0.72$ MPa m$^{1/2}$). Again, these values indicate a reasonable agreement between observations and calculations.

It should be noted that, from Fig. 12, the COD 1.35 mm behind the crack tip is approximately 2.6 μm, which is larger than the 1.7 μm value mentioned above. This difference is probably due to the fact that the CODs were measured at different crack lengths.

During the examination by optical and scanning electron microscopy, only limited evidence was seen for the existence of a microcracking zone at the crack tip or forming a wake beside the crack faces. This tended to form in the narrow region between TiB_2 grains. Support for the concept of microcracking was produced by the micrographs of the fracture surfaces (Figs 5 and 6), but observations of the crack path during SENB tests did not enable quantification of the size and extent of such a zone as might have been expected. In some micrographs (e.g. Fig. 5) there is an indication that during fabrication the BN plates were aligned parallel to the larger and stiffer TiB_2 facets. This would help explain some aspects of the tortuosness of crack paths and the relatively limited extent of microcracking. The BN/AlN phase, in which it was thought the microcracks would appear, complicated the procedure due to its inability to polish smooth. The lack of any substantial microcracking zone cannot be taken as evidence for its non-existence, as the methods used may not have been sensitive enough to distinguish the presence of such a zone. What the observations have shown is that crack interface bridging is occurring, and this could be contributing to the crack growth resistance found in this material.

3.1.2. Fracture tests

Fig. 13 shows the R-curves obtained from both SENB

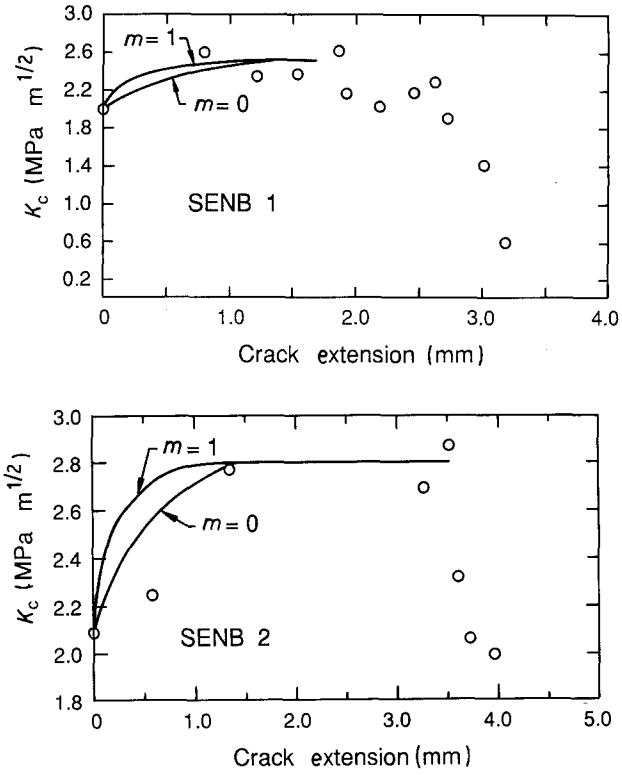

Figure 13 R-curves generated from load deflection data similar to that shown in Fig. 1 using the SENB geometry. Predictions based on Equation 4 are drawn through the data. Results shown for two SENB tests.

specimens, and demonstrates an increase in fracture resistance of the material as the crack propagates. Also evident is a pronounced drop in fracture resistance at approximately 1 mm from the specimen back face. This is thought to be due to back-face interactions affecting propagation, and will be discussed below. The graphs illustrate the curves predicted by Equation 4a–c; however accurate comparison is hampered by a lack of data points during the early stages of crack propagation. The large scatter in the results is due to an inability accurately to measure the crack-tip position, but the data are sufficient to show the general rise and then fall in the material's fracture resistance.

Application of Equations 5 and 6 to the observed data of SENB No. 2 with $m = 0$ (i.e. constant stress function over the interaction length) leads to the theoretical value of

$$u^* = 1.09\ \mu\text{m (c.f. observed } u^* = 1.7\ \mu\text{m)}$$
$$p^* = 7.92\ \text{MPa (with } u^* = 1.7\ \mu\text{m)}$$
$$= 12.35\ \text{MPa (with } u^* = 1.09\ \mu\text{m)}$$
$$p^*u^*/(m+1) = 13.5\ \text{J m}^{-2}$$

This quantity, $p^*u^*/(m + 1)$, represents the work/unit area to separate the bridges across the fracture plane and the value obtained here is comparable with typical fracture-surface energies.

Similar calculations for SENB No. 1 yield

$$u^* = 1.06\ \mu\text{m}$$
$$p^* = 5.37\ \text{MPa (with } u^* = 1.7\ \mu\text{m)}$$
$$= 8.61\ \text{MPa (with } u^* = 1.06\ \mu\text{m)}$$

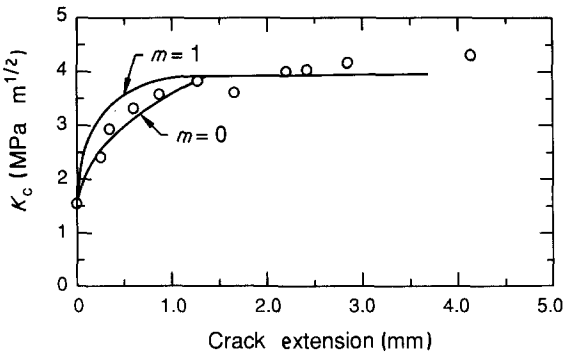

Figure 14 R-curve generated using the double cantilever beam (DCB) geometry specimen.

and $p^*u^*/(m + 1) = 9.13\ \text{J m}^{-2}$. Note that the critical crack growth for ligamentary rupture observed in the SEM, $\Delta c^* = 1.35$ mm, corresponds very closely to the value of crack growth at which the fracture resistance reaches its plateau (Fig. 13).

3.2. Double cantilever beam

3.2.1. Fracture test

Fig. 14 shows the R-curve obtained from the DCB specimen. As with the SENB specimens, we can see the increase in fracture resistance with crack growth. In this case the initial toughness is lower and the toughening increment is much greater than seen with the SENB specimens. This leads us to believe that there are geometry-related aspects to the toughening mechanism occurring within this material.

The graph shows the curves predicted by Equation 4a–c for a number of exponent values, m. These curves give a closer correspondence to the measured DCB data than with the SENB geometry. This reflects the greater accuracy with which the crack length was measured via the specimen compliances. It would be unwise, though, to predict the stress-separation function $p(u)$ based on these results, as this function is only a guide to the mechanisms operating. Thus these data should only be used to give an indication of the model's viability.

Using the observed values of Δc^* and d from SENB No. 2, application of Equations 5 and 6 to the DCB data yields (again with $m = 0$)

$$u^* = 0.8\ \mu\text{m}$$
$$p^* = 18.68\ \text{MPa (with } u^* = 1.7\ \mu\text{m)}$$
$$= 39.7\ \text{MPa (with } u^* = 0.8\ \mu\text{m)}$$

and $p^*u^*/(m + 1) = 31.76\ \text{J m}^{-2}$. As with the SENB samples, the observed value of Δc^* corresponds closely to the point at which the plateau fracture resistance is reached, although the DCB values continue to rise slowly after 1.35 mm, again indicating the possibility of geometry effects. Note that these values were obtained using observations from the SENB data and thus should only be used qualitatively.

4. Discussion

Researchers [5, 6] have contended that the interaction

of the propagating crack with a microcracking wake is responsible for the increasing fracture resistance of brittle materials. This work has shown limited evidence to support this theory, as the investigative methods used may not have been sensitive enough to detect microcracks. Although the scanning electron micrographs of Figs 4 and 5 illustrate the flake-like nature of the BN/AlN matrix and strongly suggest that a localized microcracking zone will be formed by cleavage within the matrix, only limited supporting evidence for this idea was seen during the fracture tests. This may have been a consequence of BN flake alignment parallel to the larger TiB_2 grain facets during fabrication. Thus, all that can be said is that although slight supporting evidence has been formed, the microcracking theory of R-curve behaviour is as yet unproven.

Instead this work has produced definite evidence to support the theory of crack–interface bridging [2, 8, 10]. The micrographs show two major sources of restraining forces behind the crack tip: (i) ligamentary bridges; and (ii) frictional interlocks. These forces act against the applied load and have the effect of lowering the net stress intensity factor seen by the crack tip. As the crack propagates, the number of bridging sites will increase and the apparent material fracture resistance will grow larger. This will continue until the equilibrium number of bridging sites is formed, that is, when those most distant from the crack tip rupture. When this occurs, the materials fracture resistance remains constant. This behaviour was seen in fracture tests performed on the material. Both DCB and SENB geometries gave an increase in fracture resistance with crack growth, with the graphical Δc^* being similar to the interaction length seen under the SEM. The plot of crack profile against distance from crack tip also supports the idea of crack–interface tractions forming within an interaction zone behind the crack tip.

The formation of the bridging sites was promoted due to the microstructure of the material investigated. Swanson's observations [2, 15] of crack bridging were performed on materials such as granite and coarse-grained alumina. These substances, with their large grains and (in the case of granite) a multiphase structure, prevent the crack from progressing directly through the material. Instead the crack is forced to deviate substantially from the propagation line and thus produces a macroscopically jagged crack path. Likewise, the material investigated in this work has a microstructure which is suited for producing a tortuous crack path. The large grains of TiB_2 surrounded by a matrix containing flake-like BN guide the crack and produce its jagged path. This in turn allows crack-bridging sites to be more easily formed than if the crack propagated without deviation through the material. This implies that R-curve behaviour is dependent more upon the microstructure than the material itself. Thus finer-grained materials would be anticipated to show less crack-growth resistance than coarse-grained, due to increased difficulty in producing bridging sites which remain active far behind the crack tip. The sites would remain active for a shorter distance behind the crack tip as the critical COD needed to destroy them would be small. So a fine-grained material should show a decreased value of T_∞ and Δc^* compared with the corresponding coarse-grained material. This behaviour has been seen by Knehans and Steinbrech [13] in Al_2O_3 SENB specimens of differing grain size.

As mentioned above, it should be noted that the crack deviations produced by the microstructure cause the crack propagation to change from pure mode I to a combination of modes. This would modify the stress intensity factor at the crack tip. It is uncertain what precise effect the crack deviations would have upon the system, other than to add to the material toughness through increased crack path, but this problem requires further investigation in order to gain an understanding of the mechanics of the propagating crack.

Generally, the fracture toughness tests performed on the TiB_2/BN/AlN material supported the crack–interface bridging model. The calculations performed on both specimen geometries using the theory developed by Mai and Lawn [14] give values for the work/unit area to separate the bridges that are comparable to typical fracture surface energies. However these calculations, together with the comparison of K_{Ic} data points with R-curves predicted by the theory, should only be used qualitatively to estimate the applicability of the theory. On this basis the theory shows promise, considering the possible inaccuracies in measuring the position of the crack tip within this material. Further work is required to refine the theory, in particular the form of the restraining force $p(u)$ and the effect it has upon the COD.

Further work should also be done on increasing the accuracy with which the crack tip is measured. Two methods were used during the course of this work. The first was to examine the wedged crack under an optical microscope, which necessitated the unloading of the specimen and removal from the mount (remounting was aided by the use of guide marks), a procedure which was unwieldy. Observation of the crack tip was hampered by the microstructure and led to an estimate of tip position based on the point at which the crack was no longer visible. This may have produced a sizeable error, which is reflected in the wide scatter of our data points for the SENB specimens. However, it should be noted that some materials are more amenable to the optical methods than ours, thus this method should not be dismissed. The second method, used for the DCB specimen, relied on compliance measurements for an estimate of crack position, and from the results obtained it seems to be a more accurate method. However the effect of possible microcracking on the specimen compliance and the crack-tip bridging region is not taken into account due to uncertainties in the volume fraction of microcracks and the modification they produce on the compliance on the role of the bridging stresses.

During the course of this work, it was seen that the fracture toughness measurements for various specimen geometries were different (as predicted by Mai and Lawn [14]). Figs 13 and 14 illustrate this point with the values of T_0 and T_∞ being dramatically

different between the DCB and SENB specimens. Whilst the variation in the method of crack-tip measurement would certainly contribute to this difference, we cannot ignore geometry effects when we have bridging zones of the order of millimetres, a substantial fraction of the possible crack propagation length.

A very interesting effect seen in both SENB specimens was the pronounced drop in the value of K_{Ic} towards the end of the test, the decrease occurring when the visually defined crack tip was approximately 1 mm from the back face in both specimens. Similar behaviour has been observed by Sakai and Inagaki [24] in experiments performed on a polygranular graphite material: these authors obtained a well-defined 'rising R-curve' behaviour but then found the experimentally determined value of K_{Ic} to decrease slowly after reaching its plateau value. This decrease occurred over a crack extension range of approximately 10 mm, as compared with the rather abrupt drop (range $\simeq$ 0.6 mm) seen in our data. Sakai and Inagaki [24] attribute the falling R-curve behaviour to the interaction of the microcrack process zone with the back face of the specimen, an idea that is considered more fully below. The origin of the falling R-curve behaviour in our material is possibly due to a combination of factors. Firstly, as the crack nears the back face, the remaining uncracked material acts as a 'hinge' around which the cracked specimen halves can rotate. This would increase the COD close to the crack tip and thus decrease the size of the interaction zone in which the bridging sites are active. The result would be a lowering of the crack-growth resistance, as evidenced in the graphs. However, this decrease should take place relatively slowly, becoming more obvious as the crack nears the back face. The hinge theory does not fully explain the dramatic drop in K_{Ic} approximately 1 mm from the back face, thus this is not considered to be the sole explanation for this effect.

Another possible contribution to this toughness decrease is from the interaction of microcracking ahead of the crack tip with the back face. Knehans and Steinbrech [13] support the existence of a process zone of microcracks ahead of the crack tip which dissipate energy and thus contribute to the material's crack-growth resistance. This zone arises from the superposition of crack-tip stresses with residual stresses, and will propagate ahead of the advancing crack tip.

As the crack advances the process zone will eventually reach the back face. At this point it has no further undamaged material into which it can propagate under the action of the applied load. Thus the load is now being carried solely by the microcracked material within this damaged zone. This could cause an 'oversaturation' in the microcrack density ahead of the crack tip which would lower the specimen's crack growth resistance.

Although the theories mentioned above could contribute to the observed drop in crack-growth resistance, there is an alternative explanation for this effect which is more likely. Swanson in his studies of Westerly granite [unpublished data] determined by ultrasonic means that ahead of the visually defined crack tip was a region of damaged material. He postulated that the crack tip was in fact at the front of this region and the crack faces were kept closed by the ligamentary bridging and geometrical interlocking outlined earlier.

For this work, Swanson's observations imply that the actual crack tip was ahead of that determined by optical means (an idea previously mentioned as a possible source of error in the results). Therefore the dramatic decrease in crack-growth resistance seen in our samples could be evidence that the actual crack tip has reached the back face, but with the specimen still being held together by the crack–interface tractions. The rupturing of these tractions will require an input of energy, but of a lower order than that needed to propagate the crack. Thus the material's crack-growth resistance appears to decrease whilst the visually defined crack tip propagates towards the back face. Again this raises questions as to the accuracy of methods used to define the crack-tip position, particularly in materials prone to microcracking.

5. Conclusions

This work, together with that of other researchers referenced here, leads to the conclusion that crack–interface bridging is evident in a variety of materials. Restraining forces in the form of friction interlocks and ligamentary bridging were seen and were a major contribution to the R-curve behaviour found in the TiB_2/BN/AlN material studied, but limited evidence of material toughening through a microcrack zone and wake was found. Undesirable geometry and material effects were seen in the fracture data, suggesting a need to re-evaluate the application of linear elastic fracture mechanics (LEFM) theory to materials similar to that studied here and to develop alternative methods of fracture testing.

Acknowledgements

We wish to thank R. J. Preece of Leigh-Mardon Pty Ltd for providing the specimen material, and L. R. F. Rose for helpful discussions. This work was performed at CSIRO Division of Materials Science and Technology.

References

1. J. F. KNOTT, "Fundamentals of Fracture Mechanics" (Butterworth, 1973) ch. 4 & 5.
2. P. L. SWANSON, C. J. FAIRBANKS, B. R. LAWN, Y.-W. MAI and B. J. HOCKEY, *J. Amer. Ceram. Soc.* **70** (1987) 279.
3. R. M. L. FOOTE, B. COTTERELL and Y.-W. MAI, in "Fracture Toughness and Fracture Energy of Concrete", edited by F. H. Wittman (Elsevier, Amsterdam, 1986) p. 535.
4. P. L. SWANSON, PhD thesis, University of Colorado, 1984.
5. A. G. EVANS and K. T. FABER, *J. Amer. Ceram. Soc.* **67** (1984) 255.
6. F. E. BURESCH, *Sci. Ceram.* **12** (1983) 513.
7. A. G. EVANS and R. M. CANNON, *Acta Metall.* **34** (1986) 761.
8. M. FREIDMAN, J. HARDIN and G. ALANI, *Int. J. Rock. Mech. Min. Sci.* **9** (1972) 757.

9. M. RUHLE, N. CLAUSSEN and A. H. HEUER, *J. Amer. Ceram. Soc.* **69** (1986) 195.
10. A. G. EVANS and Y. FU, *Acta Metall.* **33** (1985) 1525.
11. M. RUHLE, A. G. EVANS, R. M. McMEEKING, P. G. CHARALAMBIDES and J. W. HUTCHINSON, *ibid.* **35** (1987) 2701.
12. P. G. CHARALAMBIDES and R. M. McMEEKING, *J. Amer. Ceram. Soc.* **71** (1988) 465.
13. R. KNEHANS and R. STEINBRECH, *Sci. Ceram.* **12** (1983) 613.
14. Y.-W. MAI and B. R. LAWN, *J. Amer. Ceram. Soc.* **70** (1987) 289.
15. P. L. SWANSON, in "Advances in Ceramics" 22 (American Ceramics Society, Columbus, Ohio, 1988) p. 135.
16. R. F. COOK, in "Advanced Structural Ceramics", edited by P. F. Becher, M. V. Swain and S. Somiya (Materials Research Society, Pittsburgh, USA, 1987) p. 199.
17. B. S. MAJUMDAR, A. R. ROSENFIELD and W. H. DUCKWORTH, *Engng Fract. Mech.* **31** (1988) 683.
18. D. S. DUGDALE, *J. Mech. Phys. Solids* **8** (1960) 100.
19. M. K. BANNISTER, M. V. SWAIN, *Ceram. Int.* **15** (1989) 375.
20. *Idem., ibid.* **16** (1990) 77.
21. S. J. BURNS and M. V. SWAIN, *J. Amer. Ceram. Soc.* **69** (1986) 226.
22. B. R. LAWN, D. B. MARSHALL and A. H. HEUER, *Comm. Amer. Ceram. Soc.* **67** (1984) 253.
23. H. R. TADA, "The Stress Analysis of Cracks Handbook", 2nd edn (Del Research Corporation, Hellertown, Pennsylvania, 1985) p. 3.7a.
24. M. SAKAI and M. INAGAKI, *J. Amer. Ceram. Soc.* **72** (1989) 388.
25. S. J. BENNISON and B. R. LAWN, *Acta Metall.* **37** (1989) 2659.

Received 6 September 1990
and accepted 28 February 1991